Journal of Saudi Chemical Society (2020) **24**, 407–416

King Saud University

Journal of Saudi Chemical Society

www.ksu.edu.sa
www.sciencedirect.com

ORIGINAL ARTICLE

TiO_2 thin films sensitization with natural dyes extracted from *Bactris guineensis* for photocatalytic applications: Experimental and DFT study

Carlos Diaz-Uribe [a,*], William Vallejo [a], Eduardo Romero [a], M. Villareal [a], M. Padilla [a], N. Hazbun [a], Amner Muñoz-Acevedo [b], Eduardo Schott [c,e], Ximena Zarate [d,*]

[a] *Grupo de Investigación en Fotoquímica y Fotobiología Programa de Química. Facultad de Ciencias Básicas Universidad del Atlántico Carrera 30 # 8-49 Puerto Colombia, Atlántico, Colombia*
[b] *Grupo de Investigación en Química y Biología, Universidad del Norte. Kilómetro 5 vía Puerto Colombia, Barranquilla, Colombia*
[c] *Departamento de Química Inorgánica, Facultad de Química, Pontificia Universidad Católica de Chile, Avenida Vicuña Mackenna, 4860 Santiago, Chile*
[d] *Instituto de Ciencias Químicas Aplicadas, Theoretical and Computational Chemistry Center, Facultad de Ingeniería, Universidad Autónoma de Chile, Av. Pedro de Valdivia 425, Santiago, Chile*
[e] *Millennium Nuclei on Catalytic Processes towards Sustainable Chemistry (CSC), Chile*

Received 26 November 2019; revised 11 March 2020; accepted 16 March 2020
Available online 26 March 2020

KEYWORDS

TiO_2;
Natural sensitizer;
Anthocyanin;
DFT

Abstract TiO_2 thin films, sensitized by an anthocyanins-rich extract of a common species found in the Colombian Caribbean region (*Bactris guineensis* fruits), were used for the photocatalytic degradation of methylene blue. The sensitization process was verified by diffuse reflectance spectroscopy (DRS). The qualitative and quantitative analyses of the anthocyanins were carried out using high-performance liquid chromatography with photodiode array detection (HPLC-DAD), which provided the total content anthocyanin equivalent to delphinidin chloride (TAEDC) per mL of the extract, of 10.0 ± 0.8 μg TAEDC/mL. Here, three main anthocyanins were identified, being cyanidin-3-rutinoside the most abundant constituent (*ca.* 76%). The interaction of the dyes with a TiO_2 slab model and their adsorption energies were determined through computational simulations. In addition, the molecular modelling evidenced that the sensitization of the semiconductor

* Corresponding authors.
E-mail addresses: carlosdiaz@mail.uniatlantico.edu.co (C. Diaz-Uribe), ximena.zarate@uautonoma.cl (X. Zarate).
Peer review under responsibility of King Saud University.

Production and hosting by Elsevier

https://doi.org/10.1016/j.jscs.2020.03.004

improved the light absorption in the visible range of the spectrum. As a final point, the photocatalytic test showed that the photocatalytic activity increased 26% for TiO_2/*B. guineensis* thin films under visible radiation respect to bare TiO_2.

1. Introduction

Heterogeneous photocatalysis is considered a promising and effective way to remove organic pollutants from aquatic systems [1]. For this purpose, metal oxides (*e.g.* Titanium dioxide (TiO_2), zinc oxide (ZnO), and iron oxide have been widely employed [2]. Currently, titanium dioxide (TiO_2) is one of the most studied semiconductors for photocatalytic applications, because it is harmless to the environment, shows thermal and chemical/physical stability and exhibits photocatalytic properties under UV irradiation. Nonetheless, raw TiO_2 has some drawbacks for practical applications such as low quantum efficiency in the generation of charge-carrier, as well as the fact that it is only active under UV irradiation [3,4]. Over decades, different strategies have been implemented to address these issues and improve the TiO_2 photoactivity: (i) synthetize micro- and nano-structures (*e.g.*, spheres and three-faceted pyramids, etc.) [5,6], (ii) metal and non-metal doping [7–9], (iii) noble and/or transition metal deposition [10,11], (iv) coupling to other semiconductors [12], and (v) sensitization [13,14]. Among these, different synthetic dyes are reported as sensitizers of TiO_2, *e.g.*, ruthenium complex, porphyrins, phthalocyanines and chlorines. However, these dyes are recalcitrant substances, difficult to degrade by conventional physical–chemical processes in wastewater treatment plants [15], becoming a serious environmental trouble due to water pollution. Therefore, the search for new/innovative sources of alternative dyes are of high interest for different research institutes and government agencies. In consequence, colored natural products (*e.g.*, chlorophylls, carotenoids, anthocyanins, flavonoids and tannins) could be a powerful choice for this field because they are (i) harmless to the environment; (ii) could be used in textile, food, cosmetic and energy industries, and, (iii) are low-priced [16,17]. In the last years, natural dyes have become an alternative to develop green strategies to support conventional water treatment technologies; thus, the scientific community is encouraged not only to use natural dyes as structural templates to synthesize derivatives (with chromophores) but also to take advantage of the vast flora that earth possesses. In Colombia, there are some plants (endemic or introduced) which contain dyes that could fulfill all the properties to be used as sensitizers of TiO_2. A validated example is the species *Syzygium cumini*, whose extract of their fruits revealed its potential as sensitizer for TiO_2, based on the report of Diaz-Uribe *et al.* [18], who attributed the photocatalytic improvement to the anthocyanins contained in the extract. Subsequently, it could be hypothesized that some plants or their parts, containing anthocyanins, would be tempting candidates (their extracts or isolated molecules) as sensitizers of TiO_2. Therefore, in the herein report, we focused our attention in dyes obtained from the palm fruit *Bactris guineensis* (*Arecaceae*), which is distributed in the tropical dry forest, between Central America and northern South America. Their fruits type "drupe" (called "corozos") are used to make diverse products (*e.g.* foods, among others). In the northern region of Colombia, the red-colorful fruits prepared by decoction, have been used to elaborate artisanal beverages, jams and wines [19,20]; the seeds are discarded as wastes. According to Osorio *et al.* [19,20], the constituents responsible of *B. guineensis* fruits red color are anthocyanins, which are different to those found in the fruits extract from *S. cumini*. In the herein work, we focused on determining the composition of the methanol extract of the fruits of the palm *Bactris guineensis*, and to establish the sensitization effects over titanium dioxide (TiO_2) electrodes for solar photocatalytic process, which, to the best of our knowledge has not been studied before.

2. Experimental

2.1. Dye extraction and HPLC analysis

The vegetal material (fresh fruits) was collected at town of Piojó, Departament of Atlántico, Colombia (geographic location: Latitude: 10°45′01″ North, Longitude: 75°06′27″, to 516 m above sea level). Collection was carried out during October and November of 2017. We used percolation process for obtaining the extract, with a methanol(HCl):water mixture [2(1 M):1)], in a solvent:sample ratio of 3:1. The reversed-phase HPLC analysis was performed by using a UHPLC with a mobile phase constituted by water/formic acid/acetonitrile solutions, details for both extraction and UHPLC procedure were reported in a recent work [21].

2.2. Photocatalyst preparation and characterization

The TiO_2 thin films were deposited by the Doctor Blade method, TiO_2 powder (Degussa, P-25) was used as reagent and besides, chemisorption was used for natural dye sensitization of TiO_2 thin films [18,22,23]. The thin films morphological properties were analyzed by scanning electron microscopy (SEM) using a scanning electron microscope (Tescan VEGA3 SB) under an excitation energy of 30 kV. The diffuse reflectance spectrophotometry analysis was performed using a Beijing Elmer Lambda 4 spectrometer equipped with an integrating sphere.

Finally, in photocatalytic process we used a batch photoreactor under visible irradiation, a solution of 25 mL of MB dye (10 ppm) was used as target solution, prior to irradiate the sample, the solution was magnetically stirred in the dark for 1 h, to guarantee the equilibrium of dye adsorption/desorption onto the TiO_2 surface. Details of the photocatalytic test are reported in a previous work [18].

2.3. Computational details

Density Functional Theory computations were employed to perform a theoretical analysis of the interaction between the

isolated anthocyanins and a TiO_2 slab model. The geometry optimizations of the electronic ground states of three anthocyanins (cyanidin-3-rutinoside, cyanidin-3-glucoside and peonidin-3-rutinoside) and also adsorbed to the $(TiO_2)_{24}$ slab, have been carried out without symmetry constrains. The long-range corrected version of the Becke-3-parameter-Lee-Yang-Parr (B3LYP) hybrid exchange–correlation functional, namely the Coulomb-attenuating method-B3LYP (CAM-B3LYP) was employed in conjunction with the basis set composed of Gaussian-type orbitals, 6-31G(d,p) for C, H and O and the LANL2DZ pseudopotential for Ti atoms [20–23]. Two anchorage configurations for the cyanidin-3-rutinoside/TiO_2 and cyanidin-3-glucoside/TiO_2 were assessed, *i.e.* bidentate mononuclear chelating and bidentate binuclear chelating. The anchor groups involved in these systems were the –OH substituents enclosed by a circle in Fig. 1. These binding modes have been reported for a wide series of dyes [12,20,24–27]. Besides, in case of peonidin-3-rutinoside, as the molecule does not hold two consecutive –OH groups, two anchorage configurations were studied using the available anchors from two different rings as shown in Fig. 1c (named as positions 1 and 2). As well, the solvent effects were modeled for all our computations using the polarizable continuum model (PCM) with a dielectric constant of 24.55 which represents ethanol [32]. The anthocyanins were anchored to the $(TiO_2)_{24}$ cluster by deprotonating the OH– substituents of the molecules and protonating the cluster surface. The selected $(TiO_2)_{24}$ slab model has been chosen for this work and for other of our published studies [33]. After the geometry optimizations, the adsorption energies (ΔE_{ads}) of the dyes on the TiO_2 model were calculated based on Eq. (1):

$$\Delta E_{ads} = \left(E_{dye} + E_{TiO2}\right) - E_{dye-TiO2} \quad (1)$$

Here, E_{dye} is the total energy of free anthocyanin, E_{TiO2} is the total energy of $(TiO_2)_{24}$ slab, and $E_{dye\text{-}TiO2}$ is the total energy of the anthocyanin-$(TiO_2)_{24}$ system. Gaussian 09 software was used for the calculations [29–31].

3. Results and discussion

3.1. Identification and quantification of anthocyanins

Fig. 2 shows the typical chromatographic profile obtained by HPLC-DAD (λ 525 nm) of MeOH/HCl extract from peel/pulp of *B. guineensis* fruits. According to this profile, three anthocyanins were identified as main components: cyanidyn-3-rutinoside (~76%), cyanidin-3-glucoside (~13%), and peonidin-3-rutinoside (~8%) (Fig. 2b). This result was in agreement to previous report for these species published by Osorio *et al.* [34], who found these three anthocyanins; however, their percentage relative amounts were different and slightly lower. In addition, the total content of anthocyanin

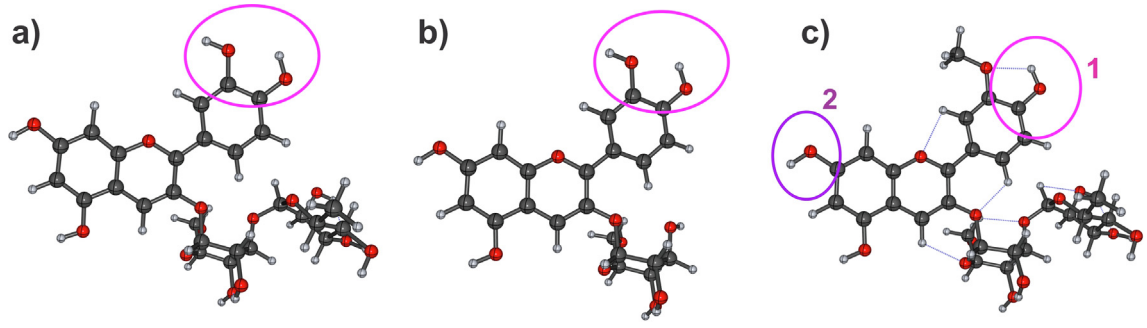

Fig. 1 Free dyes: a) Cyanidin-3-rutinoside, b) Cyanidin-3-glucoside and c) Peonidin-3-rutinoside.

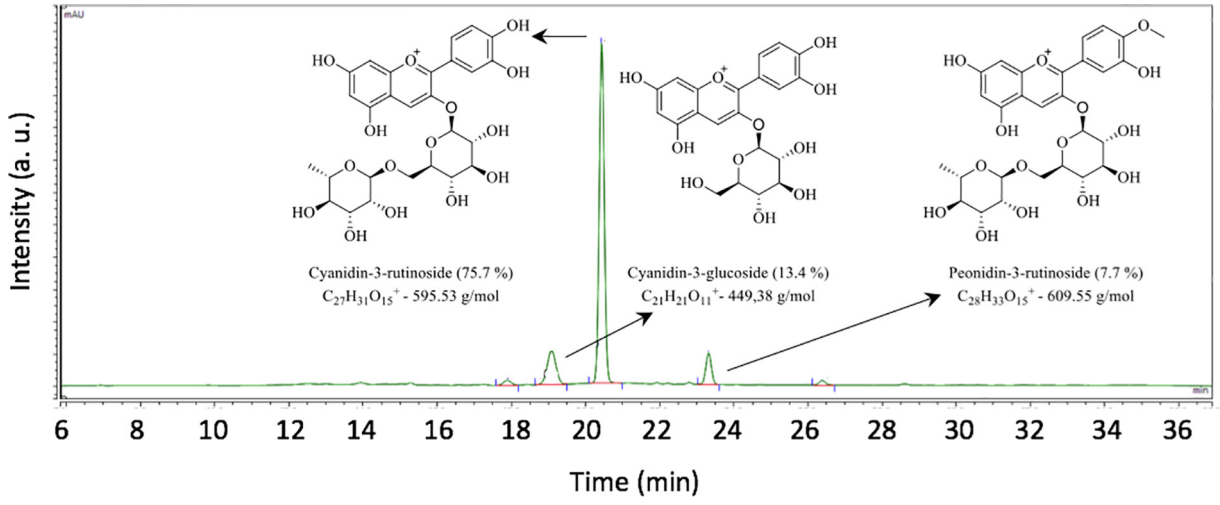

Fig. 2 Chromatographic profile by HPLC-DAD (λ 525 nm) of the total anthocyanins found in the MeOH/HCl extract of peel/pulp from *B. guineensis* fruits and, structures of the three main anthocyanins identified in MeOH/HCl extract of *B. guineensis*.

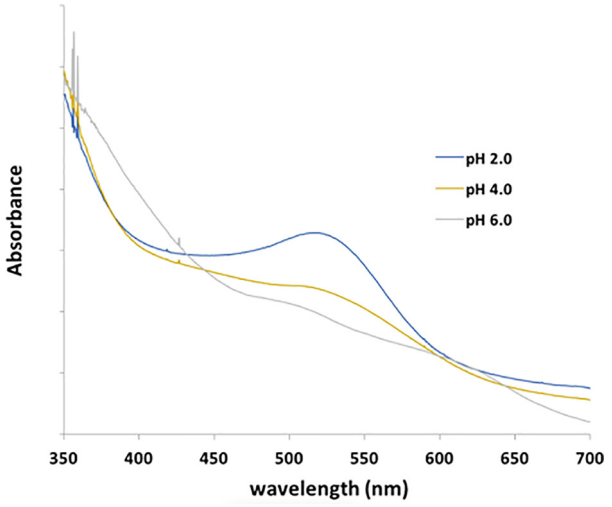

Fig. 3 UV–Vis spectra of the MeOH/HCl extract from *B. guineensis* fruits at pH values of 2, 4 and 6.

equivalent to delphinide chloride per mL (TAEDC/mL) of extract from fruit pulp/peel of *B. guineensis* was of 10.0 ± 0. 8 μg TAEDC/mL.

3.2. Optical properties of the extract

Fig. 3 shows a significant absorption band between 430 and 600 nm (at pH 2.0, with a maximum wavelength at 518 nm – visible region), this band is assigned to the flavylium cation of the anthocyanin structures found in the extract [28,35]. The change of the optical properties of the extract is pH-dependent, as their chemical structures change from flavylium cations to Carbinol pseudo-base at pH 6.0 [21]. The high absorption of light observed at pH 2.0 for the fruit extract from *B. guineensis* in the visible region, is a good indicator of its potential as a sensitizer.

3.3. Morphological characterization of the thin films

The Fig. 4 shows SEM images for both TiO_2 and TiO_2/*B. guineensis* thin films. Fig. 4 (a,b) shows that TiO_2 thin films were semi-spherical in shape and they have dense agglomeration films were formed by micro-aggregates with an average size 25 nm, the particle configuration is typical of Degussa-P25- TiO_2 using for thin films deposition [36]. After the sensitization process, the Fig. 4(c,d) shows that the average size of the films increasing to 42 nm, besides, the agglomeration increased also after natural dye sensitization. Park *et al.* reported that the agglomerates semiconductor surface could enhance the photocatalytic activity because the photogenerated charge pairs can be separated through the inter-particle charge transfer within the agglomerates [37]. These results could be a benefit for photocatalytic application due to a reduction in recombination routes.

3.4. Optical characterization of the thin films

Fig. 5 shows the diffuse reflectance spectra for TiO_2 and the TiO_2/*B. guineensis* thin films. The spectrum showed that the fruit extract from *B. guineensis* affected the optical properties of photocatalyist. Fig. 5a shows a red shift of the absorption edge towards wavelengths greater than 400 nm after sensitization process. Optical activity of TiO_2/*B. guineensis* thin films is attributed to chromophore groups (cyanidyn-3-rutinoside, cyanidin-3-glucoside and peonidin-3-rutinoside) [38,39]. The band gap energy value was determined by using the Kubelka Munk remission function and an analog to Tauc plot [40,41]:

$$(F(R_\infty)hv)^{1/2} = A(hv - E_g) \quad (2)$$

where $F(R_\infty)$ is the Kubelka Munk remission function and A is a constant. From Eq. (2), an analog to Tauc plots $(F(R_\infty)*hv)^{1/2}$ against photon energy can be constructed. Fig. 5b shows plots of $(F(R_\infty)hv)^{1/2}$ versus (hv). Results indicated that the unmodified TiO_2 had a band gap value of 3.25 eV, which agrees to reports in literature and verify that TiO_2 is active only under UV irradiation [42]. The energy value for TiO_2/*B. guineensis* thin films decreases to 2.80 eV; when the cyanidins anchored to TiO_2 surface, they improve the thin films optical properties at the visible range of the electromagnetic spectrum. Furthermore, Fig. 4b indicated that *Bactris guineensis* is an environmentally friendly and economically viable natural sensitizer source. Finally, this result is relevant to reach photocatalytic activity under visible irradiation, which is detailed in the next sections.

3.5. Computational studies

As three major anthocyanins were found in the extract, we aimed to explore how these molecules interact with the TiO_2 semiconductor. Hence, quantum mechanics calculations using the DFT method were carried out to deepen about the material photosensitization, the electronic properties as well as the molecular structures of the free anthocyanins (cyanidin-3-rutinoside, cyanidin-3-glucoside and peonidin-3-rutinoside) and adsorbed on TiO_2. As the dyes hold some available hydroxyl groups, different anchorage-binding modes to the slab model of the semiconductor were studied. Specifically, adsorption through the –OH groups in position 1 in a bidentate mononuclear and binuclear in case of the cyanidins. For peonidin-3-rutinoside, the anchorage was studied also via position 1 and we were interested in assessing the adsorption energy also through position 2 (Fig. 1, *vide supra*). To establish the binding, the hydroxo groups were deprotonated and the bonds between the O atom of the dyes (O_{dye}) and the Ti atom were generated.

The corresponding protons were transferred to the semiconductor surface upon adsorption of the dyes on the surface. The optimized geometries of the adsorbed dyes are shown if Fig. 6. The E_{ads} values were calculated using Eq. (1) and are reported in Table 1. In all cases, a stable dye/TiO_2 adsorption is observed. In general, the E_{ads} are very alike for positions 1 in the three systems (*i.e.* the bidentate mononuclear configuration for cyanidins and the through the –OH of the ring 1 in the peonidin-3-rutinoside). In case of position 2, it is observed that the Peonidin binds weaker than by position 1 as is evidenced by the decrease of the E_{ads} around 30 kcal.mol^{-1}. This indicates that certainly is more probable that the dyes bind the semiconductor through the anchor substituents on the positions 1. The molecular structures of the cyanidins adsorbed to TiO_2 show that the cyanidin with one carbohydrate in their

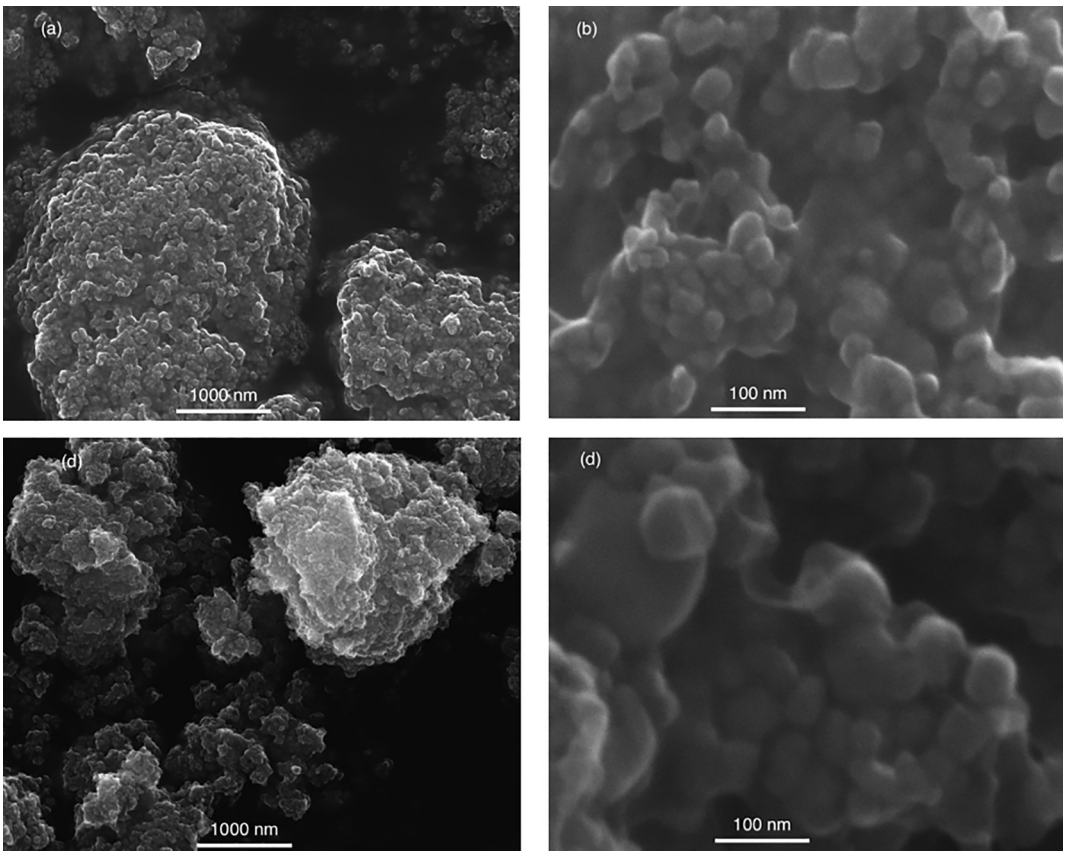

Fig. 4 SEM images for (a) TiO_2 thin films (×70000), (b) TiO_2 thin films (×1000000), (c) TiO_2/*B. guineensis* thin films (×70000), (d) TiO_2/*B. guineensis* thin films (×1000000).

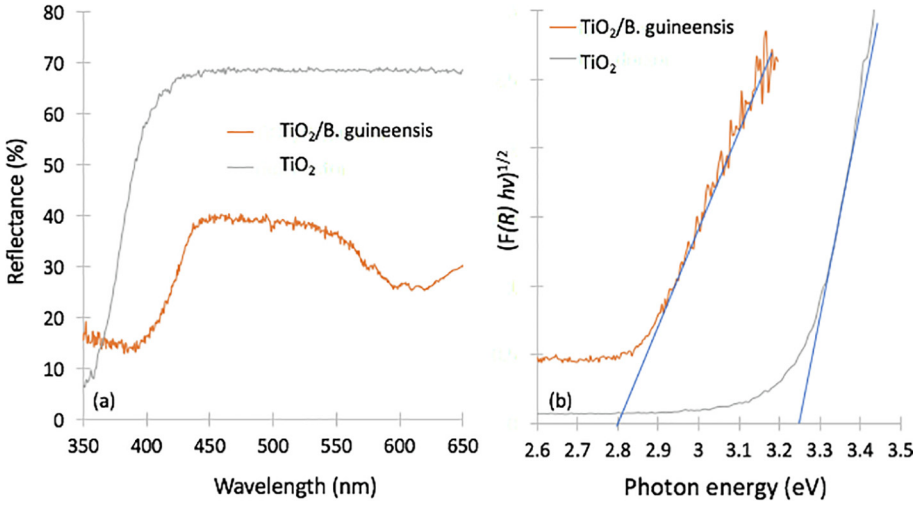

Fig. 5 a) Diffuse reflectance spectra for TiO_2 and TiO_2/*B. guineensis* thin films; and, (b) Kubelka-Munk plots and band gap energy estimation for thin films.

structure bend toward the TiO_2 more than the one with rutinoside. This is due to the steric effect of the rutinoside respect to the glucoside group.

On the other hand, regarding the energy differences between the options 1 and 2 for the peonidin-3-rutinoside anchorage modes, the computed distance $O_{(dye)}$-Ti for 1 is 1.883 Å and for 2 is 1.899 Å which are not very different. Then the crucial difference, that could contribute to the explanation of why option 1 is more stable than 2, is that the group $-OCH_3$ (specifically the oxygen atom) interacts with a Ti atom of the

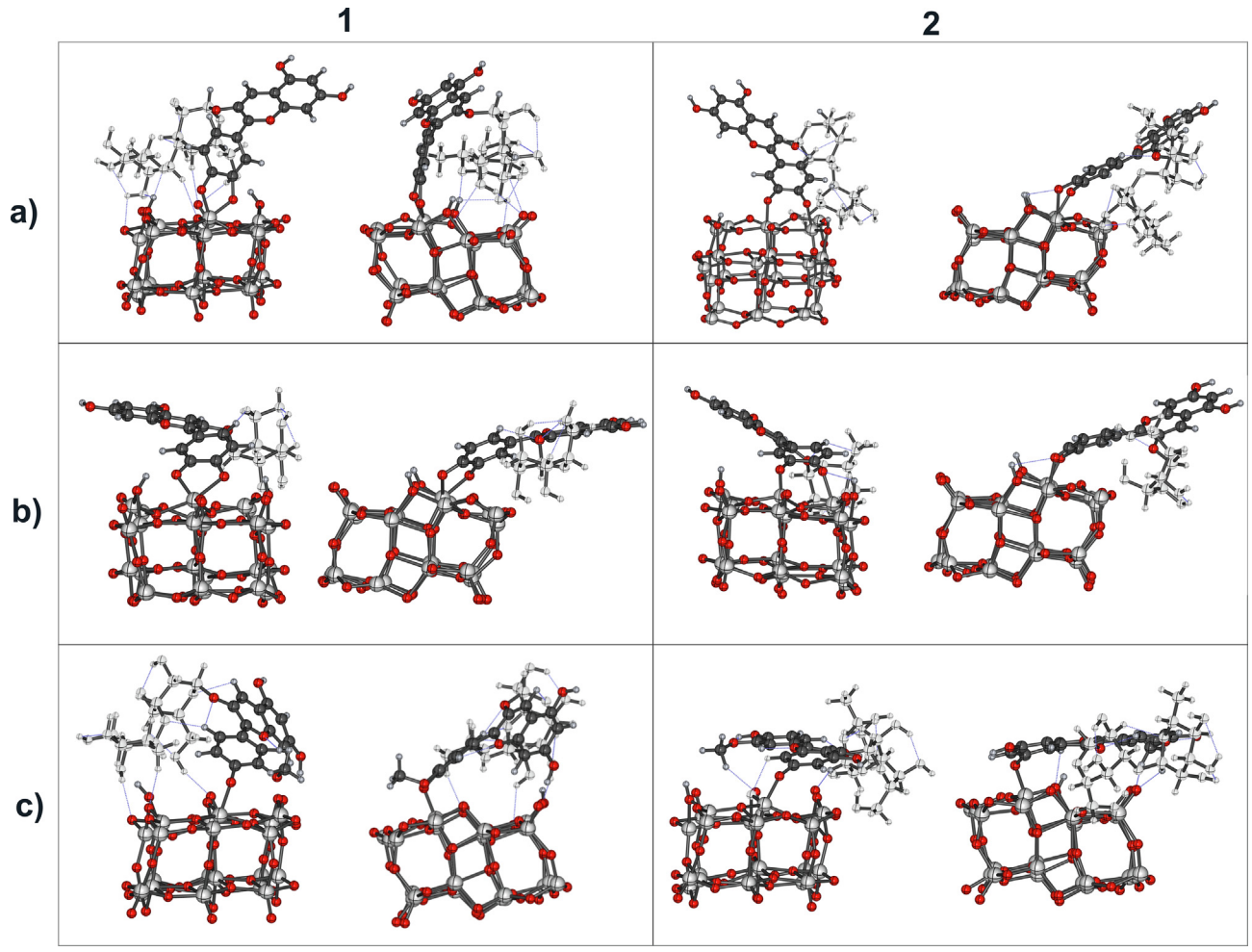

Fig. 6 Snapshots of the front and side views of the adsorption configurations (1 and 2) of the anthocyanins on TiO_2: a) cyanidin-3-rutinoside, b) Cyanidin-3-glucoside and c) Peonidin-3-rutinoside.

Table 1 Adsorption energies (E_{ads}) of the studied anthocyanins onto the TiO_2 semiconductor slab model.

	Position 1		Position 2	
	E_{ads} (kcal·mol^{-1})	E_{ads} (kJ·mol^{-1})	E_{ads} (kcal·mol^{-1})	E_{ads} (kJ·mol^{-1})
Cyanidin-3-rutinoside/TiO_2	−85.1	−351.2	−80.8	−333.4
Cyanidin-3-glucoside/TiO_2	−86.2	−355.9	−82.5	−340.7
Peonidin-3-rutinoside/TiO_2	−91.0	−375.7	−50.0	−206.1

surfaces with a distance of 1.882 Å. To assess from a computational point of view, how the sensitization improves the optical properties of the dye/TiO_2 systems, the simulation of the UV–Vis spectra through the calculation of the vertical excitations via the time-dependent DFT approaches was carried out for Cyanidin-3-rutinoside. The maximum absorption band is located at 521 nm for the bidentate mononuclear adsorption, and at 519 for the binuclear mode (Fig. 7).

This fact evidences the sensitization of the semiconductor since the TiO_2 by its own absorbs in the UV range. Also, this is successfully in good agreement with the reflectance diffuse spectra analysis.

3.6. Photocatalytic assay

Fig. 8 shows the effect of natural sensitization on MB photodegradation yield under visible irradiation after 120 min. Results highlight that when *B. guineensis* is anchored on TiO_2, the degradation of MB is higher in comparison to the bare TiO_2. MB did not show detectable degradation after visible radiation on TiO_2, these results are in agreement to higher TiO_2 band gap value. Furthermore, the Fig. 8(a) shows C_t/C_o Vs time, results shows that C_t/C_o ratio is higher (25.6%) for TiO_2/*B. guineensis* thin films than TiO_2 bare. Fig. 8(b) shows the pseudo-first order fitting for results of Fig. 8(a).

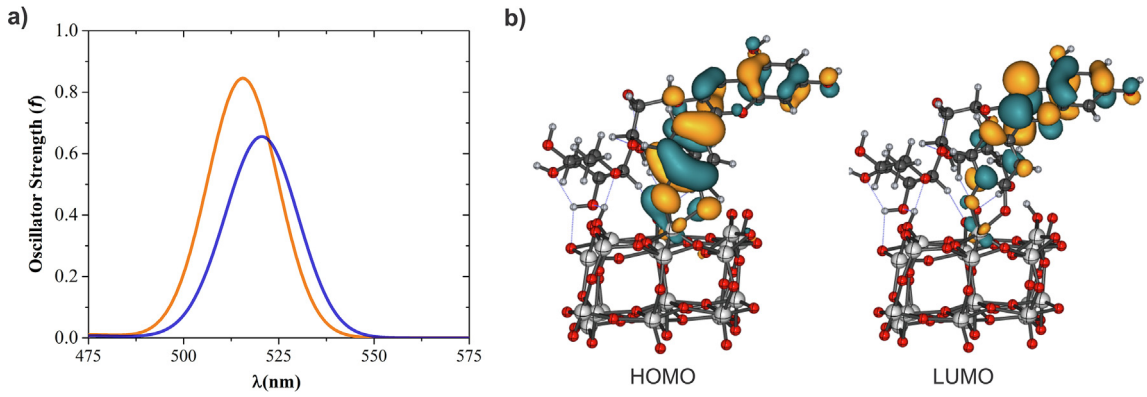

Fig. 7 a) UV–Vis spectra of the Cyanidin-3-rutinoside/TiO_2: blue line corresponds to the spectrum of the bidentate mononuclear anchorage mode and orange line corresponds to the bidentate binuclear. b) Molecular orbitals involved in these bands.

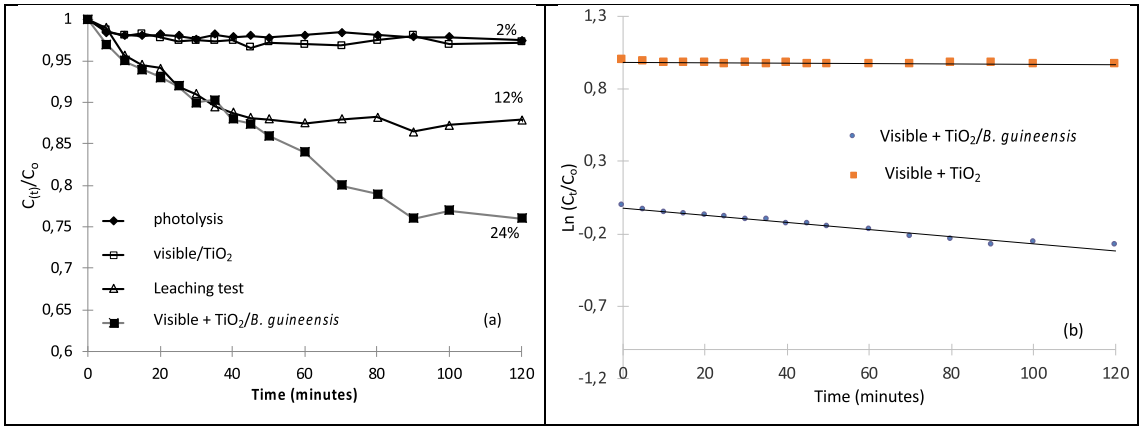

Fig. 8 (a) C_t/C_o decay for MB under visible irradiation on thin films, (b) pseudo-first order fitting for results of Fig. 8(a).

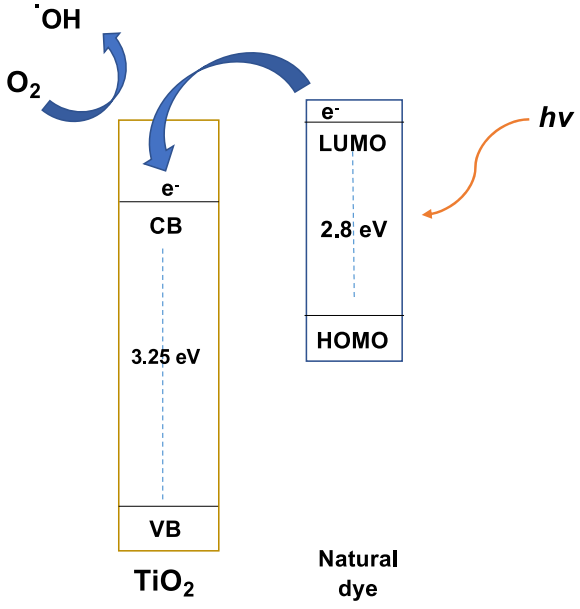

Fig. 9 Schematic illustration of TiO_2 thin film sensitization by natural dye.

According to DRS assay (Fig. 5), the mechanism of sensitization is proposed and shown in Fig. 9.

After visible irradiation, the charge carrier is transferred to TiO_2 by an electron injection from the photoexcited chromophore (cyanidins from *B. Guineensis*) to TiO_2 conduction band (Eq. (3) and Eq. (4)). The oxygen adsorbed on TiO_2 surface prevents recombination by trapping electrons, and it generates superoxide radical anions, afterwards, hydroxyl radicals can be produced according to Eq. (5) and Eq. (6). Finally, the decomposition of MB proceeds through both parallel and consecutive radical reactions (Eq. (7)) [43,44].

$$TiO_2/\text{Sensitizer} + h\nu_{(\lambda > 400\ \text{nm})} \rightarrow TiO_2/\text{Sensitizer}* \quad (3)$$

$$TiO_2/\text{Sensitizer}^+ \rightarrow TiO_2\left(e^-_{cb}\right) \quad (4)$$

$$TiO_2\left(e^-_{cb}\right) + O_{2(ad)} \rightarrow O^{\cdot -}_{2(ad)} \quad (5)$$

$$O^{\cdot -}_{2(ad)} + H_2O \rightarrow OH^{\cdot}_{(ad)} + OH^-_{(ad)} + O_{2(ad)} \quad (6)$$

$$OH^{\cdot}_{(ad)} + MB_{(ad)} \rightarrow (MB - OH^{\cdot})_{(ad)} \leftrightharpoons MB^{+}_{(ad)} + OH^-_{(ad)} \quad (7)$$

In the equations, (cb) means conduction band, (ad) means adsorbed on TiO_2 surface. Furthermore, Fig. 8 also shows results of leaching test. After 50 min reaction time, the catalyst

(TiO_2/*B. guineensis* thin film) was retired from the system, and the reaction continued without catalyst presence. The reaction mixture was then stirred by 70 min under visible irradiation. As expected, it was observed that no further conversion was obtained after the catalyst was removed from the reaction mixture. Furthermore, we tested the recyclability of the TiO_2/*B. guineensis* thin film for MB photodegradation under visible light. After the first cycle, the photodegradation yield was reduced from 24% to 17%. These features of the dyes make them potential candidates as sensitizers in Dye Sensitized Solar Cells (DSSC). In these devices, the photoexcitation of the pigment from the ground state S to the excited state S* leads to the injection of an electron into the conduction band of TiO_2 (Eq. 3–4). Then, the oxidized pigment S^+ is restored by electron transfer from the electrolyte redox pair (*e.g.* I^-/I_3^-) [45,46]. The dye cannot be regenerated if an electron is not available in the medium, and the irreversible degradation of the oxidized dye molecule competes with the regeneration by the electrolyte [47].

All results confirmed that the sensitization process was effective and demonstrated that extract from *B. guineensis* can act as an alternative sensitizer, with a remarkable increasing of the photocatalytic activity of TiO_2 in the visible range of the electromagnetic spectrum. Natural dyes are an economic and non-toxic alternative to conventional dyes used in photocatalysis.

4. Conclusions

In this work, three main anthocyanin were identified form MeOH/HCl extract of the *Bactris guinensis* fruit, which were characterized as cyanidyn-3-rutinoside (75.7%), cyanidin-3-glucoside (13.4%), and peonidin-3-rutinoside (7.7%). The pH study indicated that high pH values make the anthocyanin unstable and besides, the best spectral response was reached at pH 2.0. On the other hand, the spectroscopic and optical thin film characterization verified the sensitization process, where an improvement of the photophysical properties of TiO_2 at the visible range of electromagnetic spectrum was observed. In this sense, the best result is the increasing of 25.6% in the photocatalytic activity for TiO_2/*B. guineensis*, as bare TiO_2 did not show detectable conversion under visible light. The interaction of the dyes with a TiO_2 slab model was studied by computing the adsorption energies using quantum mechanics tools, where different anchorage configurations were assessed. We found that the $-OCH_3$ group in peonidin-3-rutinoside interacts with a Ti atom of the surface in the configuration named option 1. This fact is not observed for the other evaluated adsorption mode, which could indicate that this is mainly the responsible for the increase of the E_{ads} in this system, in comparison with the other studied systems. Otherwise, the calculations evidenced that sensitization of the semiconductor improved the light absorption properties in the visible range of the spectrum with respect to the free TiO_2, showing concordance with the reflectance diffuse spectra.

Acknowledgements

The authors would like to thank the Grants FONDECYT 11805651161416 and 1201880 ANID/FONDAP/15110019, Universidad del Atlántico (primera convocatoria interna, que otorga apoyo económico para el desarrollo de trabajos de grado en investigación formativa – nivel pregrado y postgrado). Universidad del Norte (División de Ciencias Básicas); Departamento del Atlántico (Sistema General de Regalías - Fondo de Ciencia, Tecnología e Innovación por apoyo financiero del Programa de Investigación ‘‘Implementación de proyectos de I + D (componentes Microalgas, Extractos de plantas y cadena productiva de la sábila, Producción 1,2 pro-panodiol y Plataforma informática) para promover el desarrollo y la transferencia tecnológica de cadenas productivas agroindustriales y la implementación de tecnologías de última generación para el procesamiento de biocombustibles en el departamento del Atlántico”. Millennium Science Initiative of the Ministry of Economy, Development and Tourism-Chile grant Nuclei on Catalytic Processes towards Sustainable Chemistry (CSC).

References

[1] S.A. Ansari, M.H. Cho, Growth of three-dimensional flower-like SnS2 on g-C3N4 sheets as an efficient visible-light photocatalyst, photoelectrode, and electrochemical supercapacitance material, Sustain. Energy Fuels. 1 (2017) 510–519, https://doi.org/10.1039/c6se00049e.

[2] S.A. Ansari, S.G. Ansari, H. Foaud, M.H. Cho, Facile and sustainable synthesis of carbon-doped ZnO nanostructures towards the superior visible light photocatalytic performance, New J. Chem. 41 (2017) 9314–9320, https://doi.org/10.1039/c6nj04070e.

[3] J. Schneider, M. Matsuoka, M. Takeuchi, J. Zhang, Y. Horiuchi, M. Anpo, D.W. Bahnemann, Understanding TiO 2 Photocatalysis: mechanisms and materials, Chem. Rev. 114 (2014) 9919–9986, https://doi.org/10.1021/cr5001892.

[4] A. Ayati, A. Ahmadpour, F.F. Bamoharram, B. Tanhaei, M. Mänttäri, M. Sillanpää, A review on catalytic applications of Au/TiO2 nanoparticles in the removal of water pollutant, Chemosphere 107 (2014) 163–174, https://doi.org/10.1016/J.CHEMOSPHERE.2014.01.040.

[5] S. Khameneh Asl, M. Kianpour Rad, S.K. Sadrnezhaad, M.R. Vaezi, The effect of microstructure on the photocatalytic properties of TiO2, Adv. Mater. Res. 264–265 (2011) 1340–1345, https://doi.org/10.4028/www.scientific.net/AMR.264-265.1340.

[6] T. Dikici, M. Toparli, Microstructure and mechanical properties of nanostructured and microstructured TiO2 films, Mater. Sci. Eng. A. 661 (2016) 19–24, https://doi.org/10.1016/J.MSEA.2016.03.023.

[7] C. Diaz-Uribe, W. Vallejo, W. Ramos, Methylene blue photocatalytic mineralization under visible irradiation on TiO2 thin films doped with chromium, Appl. Surf. Sci. 319 (2014) 121–127, https://doi.org/10.1016/J.APSUSC.2014.06.157.

[8] M. Humayun, F. Raziq, A. Khan, W. Luo, W. Luo, Modification strategies of TiO 2 for potential applications in photocatalysis: a critical review, Green Chem. Lett. Rev. 11 (2018) 86–102, https://doi.org/10.1080/17518253.2018.1440324.

[9] A. Kotta, S.A. Ansari, N. Parveen, H. Fouad, O.Y. Alothman, U. Khaled, H.K. Seo, S.G. Ansari, Z.A. Ansari, Mechanochemical synthesis of melamine doped TiO2 nanoparticles for dye sensitized solar cells application, J. Mater. Sci. Mater. Electron. 29 (2018) 9108–9116, https://doi.org/10.1007/s10854-018-8938-y.

[10] M. Pelaez, N.T. Nolan, S.C. Pillai, M.K. Seery, P. Falaras, A.G. Kontos, P.S.M. Dunlop, J.W.J. Hamilton, J.A. Byrne, K. O’Shea, M.H. Entezari, D.D. Dionysiou, A review on the visible light active titanium dioxide photocatalysts for environmental applications, Appl. Catal. B Environ. 125

(2012) 331–349, https://doi.org/10.1016/J.APCATB.2012.05.036.
[11] C. Díaz-Uribe, J. Viloria, L. Cervantes, W. Vallejo, K. Navarro, E. Romero, C. Quiñones, Photocatalytic Activity of Ag-TiO 2 Composites Deposited by Photoreduction under UV Irradiation, Int. J. Photoenergy. 2018 (2018) 1–8, https://doi.org/10.1155/2018/6080432.
[12] O. Ola, M.M. Maroto-Valer, Review of material design and reactor engineering on TiO2 photocatalysis for CO2 reduction, J. Photochem. Photobiol. C Photochem. Rev. 24 (2015) 16–42, https://doi.org/10.1016/J.JPHOTOCHEMREV.2015.06.001.
[13] Z. Wang, X. Lang, Visible light photocatalysis of dye-sensitized TiO2: The selective aerobic oxidation of amines to imines, Appl. Catal. B Environ. 224 (2018) 404–409, https://doi.org/10.1016/J.APCATB.2017.10.002.
[14] W. Vallejo, C. Diaz-Uribe, Á. Cantillo, Methylene blue photocatalytic degradation under visible irradiation on TiO2 thin films sensitized with Cu and Zn tetracarboxy-phthalocyanines, J. Photochem. Photobiol. A Chem. 299 (2015) 80–86, https://doi.org/10.1016/J.JPHOTOCHEM.2014.11.009.
[15] M.T. Yagub, T.K. Sen, S. Afroze, H.M. Ang, Dye and its removal from aqueous solution by adsorption: A review, Adv. Colloid Interface Sci. 209 (2014) 172–184, https://doi.org/10.1016/J.CIS.2014.04.002.
[16] W. Maiaugree, S. Lowpa, M. Towannang, P. Rutphonsan, A. Tangtrakarn, S. Pimanpang, P. Maiaugree, N. Ratchapolthavisin, W. Sang-Aroon, W. Jarernboon, V. Amornkitbamrung, A dye sensitized solar cell using natural counter electrode and natural dye derived from mangosteen peel waste, Sci. Rep. 5 15230 (2015), https://doi.org/10.1038/srep15230.
[17] H. Yang, L. Jiang, Y. Li, G. Li, Y. Yang, J. He, J. Wang, Z. Yan, H. Yang, L. Jiang, Y. Li, G. Li, Y. Yang, J. He, J. Wang, Z. Yan, Highly efficient red cabbage anthocyanin inserted TiO2 aerogel nanocomposites for photocatalytic reduction of Cr(VI) under visible light, Nanomaterials 8 (2018) 937, https://doi.org/10.3390/nano8110937.
[18] C. Díaz-Uribe, W. Vallejo, K. Campos, W. Solano, J. Andrade, A. Muñoz-Acevedo, E. Schott, X. Zarate, Improvement of the photocatalytic activity of TiO2 using Colombian Caribbean species (Syzygium cumini) as natural sensitizers: Experimental and theoretical studies, Dye. Pigment. 150 (2018) 370–376, https://doi.org/10.1016/J.DYEPIG.2017.12.027.
[19] C. Osorio, J.G. Carriazo, O. Almanza, Antioxidant activity of corozo (Bactris guineensis) fruit by electron paramagnetic resonance (EPR) spectroscopy, Eur. Food Res. Technol. 233 (2011) 103–108, https://doi.org/10.1007/s00217-011-1499-4.
[20] M.B. Rojano, I. Isabel, C. Zapata, C. Farid, B. Cortes, Anthocyanin stability and the oxygen radical absorbance capacity (ORAC) values of Corozo aqueous extracts (Bactris guineensis), 2012. http://scielo.sld.cu (accessed May 13, 2019).
[21] C. Diaz-Uribe, W. Vallejo, G. Camargo, A. Muñoz-Acevedo, C. Quiñones, E. Schott, X. Zarate, Potential use of an anthocyanin-rich extract from berries of Vaccinium meridionale Swartz as sensitizer for TiO2 thin films – An experimental and theoretical study, J. Photochem. Photobiol. A Chem. 384 (2019), https://doi.org/10.1016/J.JPHOTOCHEM.2019.112050 112050.
[22] C. Quiñones, J. Ayala, W. Vallejo, Methylene blue photoelectrodegradation under UV irradiation on Au/Pd-modified TiO2 films, Appl. Surf. Sci. 257 (2010) 367–371, https://doi.org/10.1016/J.APSUSC.2010.06.079.
[23] A.I. Kontos, A.G. Kontos, D.S. Tsoukleris, M.-C. Bernard, N. Spyrellis, P. Falaras, Nanostructured TiO2 films for DSSCS prepared by combining doctor-blade and sol–gel techniques, J. Mater. Process. Technol. 196 (2008) 243–248, https://doi.org/10.1016/J.JMATPROTEC.2007.05.051.
[24] T. Yanai, D.P. Tew, N.C. Handy, A new hybrid exchange–correlation functional using the Coulomb-attenuating method (CAM-B3LYP), Chem. Phys. Lett. 393 (2004) 51–57, https://doi.org/10.1016/j.cplett.2004.06.011.
[25] P.J. Hay, W.R. Wadt, Ab initio effective core potentials for molecular calculations. Potentials for the transition metal atoms Sc to Hg, J. Chem. Phys. 82 (1985) 270–283, https://doi.org/10.1063/1.448799.
[26] P.J. Hay, W.R. Wadt, Ab initio effective core potentials for molecular calculations. Potentials for K to Au including the outermost core orbitals, J. Chem. Phys. 82 (1985) 299–310, https://doi.org/10.1063/1.448975.
[27] W.R. Wadt, P.J. Hay, Ab initio effective core potentials for molecular calculations. Potentials for main group elements Na to Bi, J. Chem. Phys. 82 (1985) 284–298, https://doi.org/10.1063/1.448800.
[28] H. Horbowicz, M. Kosson, R. Grzesiuk, A. Debski, Anthocyanins of fruits and vegetables-their occurrence, analysis and role in human nutrition, Veg. Crop. Res. Bull. 68 (2008) 5–22, https://doi.org/10.2478/v10032-008-0001-8.
[29] X. Zarate, S. Schott-Verdugo, A. Rodriguez-Serrano, E. Schott, The nature of the donor motif in acceptor-bridge-donor dyes as an influence in the electron photo-injection mechanism in DSSCs, J. Phys. Chem. A. 120 (2016) 1613–1624, https://doi.org/10.1021/acs.jpca.5b12215.
[30] X. Zarate, M. Saavedra-Torres, A. Rodriguez-Serrano, T. Gomez, E. Schott, Exploring the relevance of thiophene rings as bridge unit in acceptor-bridge-donor dyes on self-aggregation and performance in DSSCs, J. Comput. Chem. 39 (2018) 685–698, https://doi.org/10.1002/jcc.25136.
[31] X. Zarate, F. Claveria-Cadiz, D. Arias-Olivares, A. Rodriguez-Serrano, N. Inostroza, E. Schott, Effects of the acceptor unit in dyes with acceptor–bridge–donor architecture on the electron photo-injection mechanism and aggregation in DSSCs, Phys. Chem. Chem. Phys. 18 (2016) 24239–24251, https://doi.org/10.1039/C6CP04662B.
[32] W. Sang-aroon, S. Saekow, V. Amornkitbamrung, Density functional theory study on the electronic structure of Monascus dyes as photosensitizer for dye-sensitized solar cells, J. Photochem. Photobiol. A Chem. 236 (2012) 35–40, https://doi.org/10.1016/J.JPHOTOCHEM.2012.03.014.
[33] T. Gomez, F. Jaramillo, E. Schott, R. Arratia-Pérez, X. Zarate, Simulation of natural dyes adsorbed on TiO2 for photovoltaic applications, Sol. Energy. 142 (2017) 215–223, https://doi.org/10.1016/J.SOLENER.2016.12.023.
[34] C. Osorio, B. Acevedo, S. Hillebrand, J. Carriazo, P. Winterhalter, A.L. Morales, Microencapsulation by spray-drying of anthocyanin pigments from Corozo (Bactris guineensis) fruit, J. Agric. Food Chem. 58 (2010) 6977–6985, https://doi.org/10.1021/jf100536g.
[35] E. Corradini, P. Foglia, P. Giansanti, R. Gubbiotti, R. Samperi, A. Laganà, Flavonoids: chemical properties and analytical methodologies of identification and quantitation in foods and plants, Nat. Prod. Res. 25 (2011) 469–495, https://doi.org/10.1080/14786419.2010.482054.
[36] L.M. Sikhwivhilu, S. Sinha Ray, N.J. Coville, Influence of bases on hydrothermal synthesis of titanate nanostructures, Appl. Phys. A. 94 (2009) 963–973, https://doi.org/10.1007/s00339-008-4877-4.
[37] Y. Park, W. Kim, D. Monllor-Satoca, T. Tachikawa, T. Majima, W. Choi, Role of interparticle charge transfers in agglomerated photocatalyst nanoparticles: demonstration in aqueous suspension of dye-sensitized TiO2, J. Phys. Chem. Lett. 4 (2013) 189–194, https://doi.org/10.1021/jz301881d.
[38] K.T. Ahliha A, F. Nurosyid, A. Supriyanto, Optical properties of anthocyanin dyes on TiO 2 as photosensitizers for application of dye-sensitized solar cell (DSSC) Related content, IOP Conf.

Ser, Mater. Sci. Eng. 33 (2018), https://doi.org/10.1088/1757-899X/333/1/012018 012018.
[39] P.I.E.L.U. Okoli, J.O. Ozuomba, A.J. Ekpunobi, Anthocyanin-dyed TiO2 electrode and its performance on dye-sensitized solar cell, Res. J. Recent Sci. 1 (2012) 22–27 (accessed September 30, 2018) http://www.isca.in/rjrs/archive/v1/i5/4.ISCA-RJRS-2012-73.php.
[40] E.L. Simmons, Relation of the diffuse reflectance remission function to the fundamental optical parameters, Opt. Acta Int. J. Opt. 19 (1972) 845–851, https://doi.org/10.1080/713818505.
[41] B.D. Viezbicke, S. Patel, B.E. Davis, D.P. Birnie, Evaluation of the Tauc method for optical absorption edge determination: ZnO thin films as a model system, Phys. Status Solidi. 252 (2015) 1700–1710, https://doi.org/10.1002/pssb.201552007.
[42] K. Madhusudan Reddy, S.V. Manorama, A. Ramachandra Reddy, Bandgap studies on anatase titanium dioxide nanoparticles, Mater. Chem. Phys. 78 (2003) 239–245, https://doi.org/10.1016/S0254-0584(02)00343-7.
[43] Z. Youssef, L. Colombeau, N. Yesmurzayeva, F. Baros, R. Vanderesse, T. Hamieh, J. Toufaily, C. Frochot, T. Roques-Carmes, S. Acherar, Dye-sensitized nanoparticles for heterogeneous photocatalysis: Cases studies with TiO2, ZnO, fullerene and graphene for water purification, Dye. Pigment. 159 (2018) 49–71, https://doi.org/10.1016/J.DYEPIG.2018.06.002.
[44] K. Ishibashi, A. Fujishima, T. Watanabe, K. Hashimoto, Quantum yields of active oxidative species formed on TiO2 photocatalyst, J. Photochem. Photobiol. A Chem. 134 (2000) 139–142, https://doi.org/10.1016/S1010-6030(00)00264-1.
[45] H. Hug, M. Bader, P. Mair, T. Glatzel, Biophotovoltaics: Natural pigments in dye-sensitized solar cells, Appl. Energy. 115 (2014) 216–225, https://doi.org/10.1016/J.APENERGY.2013.10.055.
[46] S. Shalini, R. Balasundaraprabhu, T.S. Kumar, N. Prabavathy, S. Senthilarasu, S. Prasanna, Status and outlook of sensitizers/dyes used in dye sensitized solar cells (DSSC): a review, Int. J. Energy Res. 40 (2016) 1303–1320, https://doi.org/10.1002/er.3538.
[47] S. Zhang, X. Yang, Y. Numata, L. Han, Highly efficient dye-sensitized solar cells: Progress and future challenges, Energy Environ. Sci. 6 (2013) 1443–1464, https://doi.org/10.1039/c3ee24453a.